Classifying DME vs Normal SD-OCT volumes: A review

Joan Massich*, Mojdeh Rastgoo*†, Guillaume Lemaître*†, Carol Y. Cheung*,
Tien Y. Wong†, Désiré Sidibé†, Fabrice Mériaudeau*§

*LE2I UMR6306, CNRS, Arts et Métiers, Univ. Bourgogne Franche-Comté,
12 rue de la Fonderie, 71200 Le Creusot, France
†ViCOROB, Universitat de Girona, Campus Montilivi, Edifici P4, 17071 Girona, Spain
‡Singapore Eye Research Institute, Singapore National Eye Center, Singapore
§Centre for Intelligent Signal and Imaging Research (CISIR), Electrical & Electronic Engineering Department,
Universiti Teknologi Petronas, 32610 Seri Iskandar, Perak, Malaysia
¶Corresponding author: joan.massich@u-bourgogne.fr

Abstract—

Index Terms—

I. INTRODUCTION

Eye diseases such as Diabetic Retinopathy (DR) and Diabetic Macular Edema (DME) are the most common causes of irreversible vision loss in individuals with diabetes. Just in United States alone, health care and associated costs related to eye diseases are estimated at almost $500\,$M [1]. Moreover, the prevalent cases of DR are expected to grow exponentially affecting over $300\,$M people worldwide by 2025 [2]. Given this scenario, early detection and treatment of DR and DME play a major role to prevent adverse effects such as blindness. DME is characterized as an increase in retinal thickness within 1 disk diameter of the fovea center with or without hard exudates and sometimes associated with cysts [3]. Fundus images which have proven to be very useful in revealing most of the eye pathologies [4, 5] are not as good as Optical Coherence Tomography (OCT) images which provide information about cross-sectional retinal morphology [6]. old

Many of the previous works on OCT image analysis have focused on the problem of retinal layers segmentation, which is a necessary step for retinal thickness measurements [7, 8]. However, few have addressed the specific problem of DME and its associated features detection from OCT images. Figure **??** shows one normal B-scan and two abnormal B-scans. old

Evaluation of the volumetric scan is time consuming, expensive and some pathology signs are easy to miss [9]

· coexistence of multiple pathologies [10] · OCT image acquisition has drift [10] · variability in shape, size and magnitude within the same pathology [10] · retina reflectivity (schuman 2014) [10] · inconsistent image quality (barnum 2008) [10] sik

This article is structured as follows: Background(Sect. II) offers a general idea of the methods reviwed. Materials and methods discusses data and mapping of the methodologies to our framework. Results offers (Sect. V) (a) individual results of each methodology, as well as our strategy followed to validate that our implementation complies with the results reported by the original work (b) comparative results of the best methodlogy configurations to drive our discussion. Discussion(Sect. V). Conclusion and Further work(Sect. VI). sik

II. BACKGROUND

This section reviews works straightly addressing the problem of classifying OCT volumes as normal or abnormal, regardless of the target pathology. The methods are categorized in terms of its learning strategy, namely: supervised or semi-supervised.

A. Supervised methods

Supervised classification is based on full annotated and labeled training set. In such methods the labeled training data is used to train the classifier function, which is latter used for prediction. Figure 1 describes a prevalent structure for supervised classification. The volumes undergo: (i) *Pre-processing* to reduce the natural noise of the images and correct acquisition deficiencies; (ii) *Feature detection* to quantify visual cues like appearance, texture, shape, etc. (iii) *Mapping* to determine the discrete set of elements (structures) to represent the sample to be classified (i.e.B-scan/volume); (iv) *Feature representation* to associate a descriptor for each element from the *mapping-stage*. This descriptor packages the visual cues associated to the sample. (v) *Classification*.

Venhuizen *et al.* propose a classification method to distinguish between Age-related Macular Degeneration (AMD) and normal Spectral Domain OCT (SD-OCT) volumes using Bag-of-Words (BoW) models [9]. The method detects and selects a set of keypoints at each individual B-scan. Essentially, keeping the salient points comprised at the top 3% of the vertical gradient values. Then, a texton of size 9×9 pixels is extracted around each keypoint, and Principal Component Analysis (PCA) is applied to reduce the dimension of every texton to get a feature vector of size 9. All extracted feature vectors are used to create a codebook using k-means clustering. Then, each OCT volume is represented in terms of this codebook
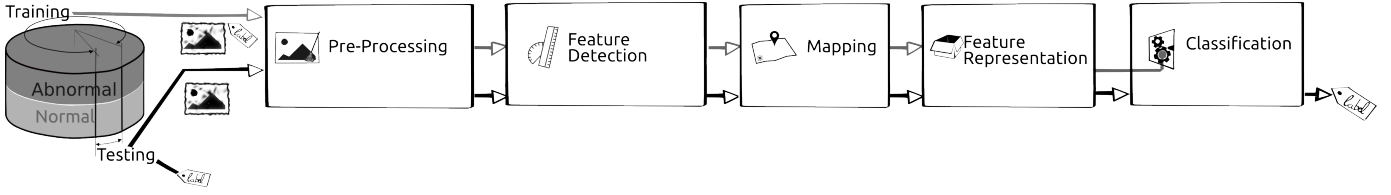
Fig. 1. Common framework

and is characterized as a histogram that captures the codebook occurrences. These histograms are used as feature vector to train a Random Forest (RF) with a maximum of 100 trees. The method is tested using a publicly available dataset of 384 OCT volumes [11], achieving an Area Under the Curve (AUC) of 0.984.

Srinivasan *et al.* [12] propose a classification method to distinguish DME, AMD and normal SD-OCT volumes. The OCT images are pre-processed by first enhancing sparsity in a transform-domain (BM3D [13]), to reduce their speckle noise, and then by flattening the retinal curvature to reduce the inter-patient variations. Histogram of Oriented Gradients (HOG) features are then extracted from multi-resolution pyramid of each pre-processed slice of a volume. These features are classified using a linear Support Vector Machines (SVM). Note that the method classifies each individual B-scan into one of three categories, i.e.DME, AMD, and normal, and then classifies a volume based on the number of B-scans in each category. This method is also tested using a publicly available dataset, composed of 45 patients equally subdivided into the three target classes. The method achieves a correct classification rate of 100%, 100% and 86.67% for normal, DME and AMD patients, respectively.

Alsaih *et al.* [14] extended Srinivasan *et al.* [12] by (i) incorporating Local Binary Patterns (LBP) to the feature detection stage; and (ii) adding PCA to the feature representation step, as proposed by Venhuizen *et al.* [9];

Lemaitre *et al.* [15] propose a method based on LBP features to describe the texture of OCT images and dictionary learning using the BoW models [16]. Note that using BoW and dictionary learning contrary to [12] the classification is performed per volume, rather than B-scan. In this method the OCT images are first pre-processed using Non-Local Means (NLM) filtering, to reduce the speckle noise. Then the volumes are mapped into discrete set of structures namely: local, when these structures correspond to patches; or global, when they correspond to volume slices or the whole volume. According to different mapping, LBP or LBP from Three Orthogonal Planes (LBP-TOP) texture features are extracted and represented (per volume) using histogram, PCA or BoW. The final feature descriptors per volumes are classified using RF classifier. This methodology was tested against Venhuizen *et al.* [9] using public and non-public datasets showing an improvement within the results by achieving a Sensitivity (SE) of 87.5% and a Specificity (SP) of 75%.

Liu *et al.* propose a methodology aiming for B-scan clas-

sification, rather than volume classification. The classification goal is to distinguish between macular pathology and normal OCT B-scan images using LBP and gradient information as attributes [10]. The method starts by aligning and flattening the images and creating a 3-level multi-scale spatial pyramid. The edge and LBP histograms are then extracted from each block of every level of the pyramid. All the obtained histograms are concatenated into a global descriptor whose dimensions are reduced using PCA. Finally a SVM with an Radial Basis Function (RBF) kernel is used as classifier. The method achieved good results in detection of OCT scan containing different pathology such as DME or AMD, with an AUC of 0.93 using a dataset of 326 OCT scans.

Albarrak *et al.* [17] propose another volumetric classification framework for differentiating AMD and normal volumes. The author propose to flatten the volume of interest (VOI) from each OCT volume as a pre-processing step and extract LBP-TOP and HOG+LBP-TOP features from individual sub-volumes within each VOI. The extracted features were concatenated into a single feature vector per OCT volume and presented in lower dimensions using PCA. Finally a Bayesian network classifier was used for classifying the volumes. Testing their proposed method and comparing with [10] using 140 OCT volumes, they achieved the highest SE and SP of 92.4% and 90.5%, respectively.

Anantrasirichai *et al.* [18] propose to detect glaucoma in OCT images based on a variety of texture measures. The images are described in terms of LBP, Gray-level co-occurrence matrix (GLCM), wavelet, granulometry, run length measures, and intensity level distributions in combination with retinal layer thickness without any pre-processing. Using PCA and linear and kernel-SVM classifier, the authors compared the performance of individual features and their combinations. Testing with rather a small dataset of 24 OCT voluems, their proposed method achieved an Accuracy (ACC) of 81.95% while using layer thickness information.

B. Semi-supervised methods

An example of semi-supervised approach for SD-OCT classification is recently proposed by Sankar. *et al.* [19]. The proposed method is based on appearance modeling of normal OCT images using Gaussian Mixture Model (GMM) and anomaly detection. The abnormal B-scans are detected as outliers to the fitted GMM and volume classification is performed based on the number of detected outliers in the volume.

This approach differs from supervised approaches since the B-scan detection method does not require a labeled training set of B-scans. This method starts by pre-processing the B-scans using resizing, flattening and denoising (NLM filter). The features are extracted by taking the intensity information of each B-scan and applying PCA to reduce their dimension. The feature space is then modeled using GMM. In the testing stage, for the new B-scan, the features are extracted in a similar way and they are classified as normal or abnormal based on their Mahalanobis distance to the GMM. Finally the volume classification is performed considering the umber of outliers (abnormal) B-scans per volume.

III. DATA

In order to compare different methodologies, the first requirement is access to a common pull of images. Despite the fact that lack of public data is a common claim within the medical image community [20], the community developing methodologies for SD-OCT imagery has public data available [11, 12], mainly gathered at *Duke University*. However this data has deficiencies that makes it unsuitable for our problem. Venhuizen *et. al.* test using a large public dataset of 384 OCT annotated volumes of AMD *vs. normal* cases. Despite the interest of testing against a large dataset, our goal remains not to detect AMD but to study the detection of DME. Srinivasan *et al.* [12] also test using a public dataset from *Duke Univeristy*, this time containing AMD, DME and *normal* volumes. However, the volumes of this dataset have been manipulated using pre-processing, realignment, cropping, etc. and there original data is not available making the dataset unsuited for our purposes.

Therefore, we use the Singapore Eye Research Institute (SERI) dataset [21] to conduct this study (see fig. 2). This dataset was acquired by the SERI, using CIRRUS TM (Carl Zeiss Meditec, Inc., Dublin, CA) SD-OCT device. The dataset consists of 32 OCT volumes (16 DME and 16 normal cases). Each volume contains 128 B-scan with resolution of 512×1024 pixels. All SD-OCT images are read and assessed by trained graders and identified as normal or DME cases based on evaluation of retinal thickening, hard exudates, intraretinal cystoid space formation and subretinal fluid.

IV. EXPERIMENTAL SETUP

The experimental set-up is summarized in table I. Where the most relevant works in Sect. II are formulated as the as the 5-steps standard classification procedure described in Fig. 1.

A. *Implementation details*

For reproductivity purposes, the experimentation described in this work can be found in [22], where the image processing and Machine Learning (ML) rapid pipeline prototyping library *Protoclass* [23] has been used to implement the methodologies in Tab. I in accordance to proposed experimentation framework. Each methodology implementation can be seen as a plug-in to experiment in [22], while references to stand-alone implementation of these methodologies can be found in Tab. I.

Fig. 2. SERI dataset description.

TABLE I
CORRESPONDENCE BETWEEN THE MOST RELEVANT METHODOLOGIES REVIEWED IN SECT. II AND THE PROPOSED EXPERIMENTAL FRAMEWORK.

Ref	Pre-processing	Features	Mapping	Representation	Classification
Venhuizen *et al.* [9, 24]		Texton	Local	BoW, PCA	RF
Srinivasan *et al.* [12, 25]	De-noise Flatten Cropped	HOG	Global		linear-SVM
Lemaitre *et al.* [15, 26]	De-noised	LBP LBP-TOP	Local Global	PCA, BoW, Histogram	RF
Alsaih *et al.* [14]	*********	LBP LBP-TOP	***** ******	PCA, BoW, *********	RF
Sankar *et al.* [19, 27]	De-noised Flatten Cropped	Pixel -intensities	Global	PCA	Mahalanobis -distance to GMM

All the repositories are publicly available and provided with tests to ensure that our implementation agrees with the results reported by the original works. [1]

B. *Evaluation*

All the experiments are evaluated in terms of SE and SP (see Eq. 1) using the Leave-One-Patient Out Cross-Validation (LOPO-CV) strategy, in line with [15]. The SE evaluates the performance of the classifier with respect to the positive class, while the SP evaluates its performance with respect to negative class.

$$ SE = \frac{TP}{TP + FN} \qquad SP = \frac{TN}{TN + FP} \qquad (1) $$

The use of LOPO-CV implies that at each round, a pair DME-normal volume is selected for testing while the remaining volumes are used for training. Subsequently, no SE or SP variance can be reported. However, LOPO-CV strategy has been adopted despite this limitation due to the reduced size of the dataset.

[1]Note that methodologies where this quality control could not had been enforced have been discarded for experimentation and only reviewed based on the results reported by the original work and compiled in Sect. II.

V. Results and Discussion

Table II shows the results obtained in terms of SE and SP, where Sankar *et. al.* achieve the best performance, revealing that DME lesions can be modeled accurately based only on a set of normal SD-OCT volumes.

VI. Conclusion and Further work

The work here presented states the relevance of developing methodologies to automatically differentiate DME *vs. normal* SD-OCT scans. This article offers an overview of the state-of-the-art methodologies and provides a public benchmarking to facilitate further studies. In this regard, there are two crucial aspects to improve the work here presented: (i) enlarge the dataset. (ii) reach out for the original authors of those methods in Sect. II that could not be included in Sect. **??** because our implementation could not be tested against the original data or we did not achieve the original results.

References

[1] S. Sharma, A. Oliver-Hernandez, W. Liu, and J. Walt, "The impact of diabetic retinopathy on health-related quality of life," *Current Opinion in Ophtalmology*, vol. 16, pp. 155–159, 2005.

[2] S. Wild, G. Roglic, A. Green, R. Sicree, and H. King, "Global prevalence of diabetes estimates for the year 2000 and projections for 2030," *Diabetes Care*, vol. 27, no. 5, pp. 1047–1053, 2004.

[3] Early Treatment Diabetic Retinopathy Study Group, "Photocoagulation for diabetic macular edema: early treatment diabetic retinopathy study report no 1," *JAMA Ophthalmology*, vol. 103, no. 12, pp. 1796–1806, 1985.

[4] M. R. K. Mookiah, U. R. Acharya, C. K. Chua, C. M. Lim, E. Ng, and A. Laude, "Computer-aided diagnosis of diabetic retinopathy: A review," *Computers in Biology and Medicine*, vol. 43, no. 12, pp. 2136–2155, 2013.

[5] E. Trucco, A. Ruggeri, T. Karnowski, L. Giancardo, E. Chaum, J. Hubschman, B. al Diri, C. Cheung, D. Wong, M. Abramoff, G. Lim, D. Kumar, P. Burlina, N. M. Bressler, H. F. Jelinek, F. Meriaudeau, G. Quellec, T. MacGillivray, and B. Dhillon, "Validation retinal fundus image analysis algorithms: issues and proposal," *Investigative Ophthalmology & Visual Science*, vol. 54, no. 5, pp. 3546–3569, 2013.

[6] Y. T. Wang, M. Tadarati, Y. Wolfson, S. B. Bressler, and N. M. Bressler, "Comparison of Prevalence of Diabetic Macular Edema Based on Monocular Fundus Photography vs Optical Coherence Tomography," *JAMA Ophthalmology*, pp. 1–7, Dec 2015.

[7] S. J. Chiu, X. T. Li, P. Nicholas, C. A. Toth, J. A. Izatt, and S. Farsiu, "Automatic segmentation of seven retinal layers in sd-oct images congruent with expert manual segmentation," *Optic Express*, vol. 18, no. 18, pp. 19 413–19 428, 2010.

[8] R. Kafieh, H. Rabbani, M. D. Abramoff, and M. Sonka, "Intra-retinal layer segmentation of 3d optical coherence tomography using coarse grained diffusion map," *Medical Image Analysis*, vol. 17, pp. 907–928, 2013.

[9] F. G. Venhuizen, B. van Ginneken, B. Bloemen, M. J. P. P. van Grisven, R. Philipsen, C. Hoyng, T. Theelen, and C. I. Sanchez, "Automated age-related macular degeneration classification in OCT using unsupervised feature learning," in *SPIE Medical Imaging*, vol. 9414, 2015, p. 94141l.

[10] Y.-Y. Liu, M. Chen, H. Ishikawa, G. Wollstein, J. S. Schuman, and R. J. M., "Automated macular pathology diagnosis in retinal oct images using multi-scale spatial pyramid and local binary patterns in texture and shape encoding," *Medical Image Analysis*, vol. 15, pp. 748–759, 2011.

[11] S. Farsiu, S. J. Chiu, R. V. O'Connell, F. A. Folgar, E. Yuan, J. A. Izatt, C. A. Toth, A.-R. E. D. S. . A. S. D. O. C. T. S. Group *et al.*, "Quantitative classification of eyes with and without intermediate age-related macular degeneration using optical coherence tomography," *Ophthalmology*, vol. 121, no. 1, pp. 162–172, 2014.

[12] P. P. Srinivasan, L. A. Kim, P. S. Mettu, S. W. Cousins, G. M. Comer, J. A. Izatt, and S. Farsiu, "Fully automated detection of diabetic macular edema and dry age-related macular degeneration from optical coherence tomography images," *Biomedical Optical Express*, vol. 5, no. 10, pp. 3568–3577, 2014.

[13] K. Dabov, A. Foi, V. Katkovnik, and K. Egiazarian, "Image denoising by sparse 3-d transform-domain collaborative filtering," *Image Processing, IEEE Transactions on*, vol. 16, no. 8, pp. 2080–2095, 2007.

[14] K. Alsaih, G. Lemaitre, J. Massich, M. Rastgoo, D. Sidibe, and F. Meriaudeau, "alsaih-2016-aug: Icpr 2016," Apr. 2016. [Online]. Available: http://dx.doi.org/10.5281/zenodo.49499

[15] G. Lemaitre, M. Rastgoo, J. Massich, S. Sankar, F. Meriaudeau, and D. Sidibe, "Classification of SD-OCT volumes with LBP: Application to dme detection," in *Medical Image Computing and Computer-Assisted Intervention (MICCAI), Ophthalmic Medical Image Analysis Workshop (OMIA)*, 2015.

[16] J. Sivic and A. Zisserman, "Video google: a text retrieva approach to object matching in videos," in *IEEE ICCV*, 2003, pp. 1470–1477.

[17] A. Albarrak, F. Coenen, and Y. Zheng, "Age-related macular degeneration identification in volumetric optical coherence tomography using decomposition and local feature extraction," in *Proceedings of 2013 International Conference on Medical Image, Understanding and Analysis*, 2013, pp. 59–64.

[18] N. Anantrasirichai, A. Achim, J. E. Morgan, I. Erchova, and L. Nicholson, "Svm-based texture classification in optical coherence tomography," in *IEEE 10th International Symposium on Biomedical Imaging (ISBI)*. IEEE, 2013, pp. 1332–1335.

[19] S. Sankar, D. Sidibé, Y. Cheung, T. Wong, E. Lamoureux, D. Milea, and F. Meriaudeau, "Classification of sd-oct volumes for dme detection: an anomaly detection approach," in *SPIE Medical Imaging*. International Society for Optics and Photonics, 2016, pp. 97 852O–97 852O.

[20] M. L. Giger, H.-P. Chan, and J. Boone, "Anniversary paper: History and status of CAD and quantitative image analysis: the role of medical physics and AAPM," *Medical physics*, vol. 35, no. 12, p. 5799, 2008.

[21] G. Lemaitre, J. Massich, M. Rastgoo, S. Sankar, D. Sidibe, . ******, . ******, . ******, and F. Meriaudeau, "srinivasan-2014-oct: Icpr 2016," Apr. 2016. [Online]. Available: *****************************

[22] J. Massich, G. Lemaitre, and M. Rastgoo, "*****************************," Apr. 2016. [Online]. Available: *****************************

[23] G. Lemaitre, "Protoclass, a rapid prototyping tool for image processing and machine learning," Apr. 2016. [Online]. Available: *****************************

[24] G. and Lemaitre, J. Massich, and M. Rastgoo, "*****************************," Feb. 2016. [Online]. Available: *****************************

[25] G. Lemaitre, J. Massich, and M. Rastgoo, "srinivasan-2014-oct: Icpr 2016," Apr. 2016. [Online]. Available: http://dx.doi.org/10.5281/zenodo.49669

[26] ——, "*****************************," Apr. 2016. [Online]. Available: *****************************

[27] ——, "*****************************," Feb. 2016. [Online]. Available: *****************************

TABLE II
SUMMARY OF THE CLASSIFICATION PERFORMANCE IN TERMS OF SE AND SP IN (%).

	Srinivasan *et al.* [12]	Venhuizen *et al.* [9]	Alsaih *et al.* [14]	Lemaitre *et al.* [15]	Sankar *et al.* [19]
SE	61.5	68.8	75.0	61.3	93.8
SP	58.8	93.8	87.5	83.8	80.0